University of South Carolina College of Engineering and Computing Mechanical Engineering Department

Nanostructured Copper Interfaces for Enhanced Boiling

Chen Li,y Zuankai Wang,y Pei-I Wang, Yoav Peles, Nikhil Koratkar, and G. P. Peterson

Nanostructured copper

DOI: 10.1002/smll.200700991

Nanostructured Copper Interfaces for Enhanced Boiling**

Chen Li,† Zuankai Wang,† Pei-I Wang, Yoav Peles, Nikhil Koratkar, and G. P. Peterson**

Phase change through boiling is used in a variety of heat-transfer and chemical reaction applications.[1–7] The state of the art in nucleate boiling has focused on increasing the density of bubble nucleation using porous structures and microchannels[8–12] with characteristic sizes of tens of micrometers. Traditionally, it is thought that nanoscale surfaces will not improve boiling heat transfer, since the bubble nucleation process is not expected to be enhanced by such small cavities.[13–15] In the experiments reported here, we observed unexpected enhancements in boiling performance for a nanostructured copper (Cu) surface formed by the deposition of Cu nanorods on a Cu substrate. Moreover, we observed striking differences in the dynamics of bubble nucleation and release from the Cu nanorods, including smaller bubble diameters, higher bubble release frequencies, and an approximately 30-fold increase in the density of active bubble nucleation sites. It appears that the ability of the Cu surface with nanorods to generate stable nucleation of bubbles at low superheated temperatures results from a synergistic coupling effect between the nanoscale gas cavities (or nanobubbles[16–18]) formed within the nanorod interstices and micrometer-scale defects (voids) that form on the film surface during nanorod deposition. For such a coupled system, the interconnected nanoscale gas cavities stabilize (or feed) bubble nucleation at the microscale defect sites. This is distinct from conventional-scale boiling surfaces, since for the nanostructured surface the bubble nucleation stability is provided by features with orders-of-magnitude smaller scales than the cavity-mouth openings.

[*] Prof. N. Koratkar, Z. Wang, Prof. Y. Peles
Department of Mechanical, Aerospace, and Nuclear Engineering
Rensselaer Polytechnic Institute
Troy, NY 12180 (USA)
E-mail: koratn@rpi.edu
Prof. G. P. Peterson, Dr. C. Li
Department of Mechanical Engineering
University of Colorado
Boulder, CO 80309 (USA)
E-mail: bud.peterson@colorado.edu
Dr. P.-I. Wang
Department of Physics, Applied Physics, and Astronomy
Rensselaer Polytechnic Institute
Troy, NY 12180 (USA)

[†] These authors contributed equally to this work.

[**] The authors acknowledge the support of the National Science Foundation under award CEBT-0721246 to G.P.P. and awards ECS 0403789 and ECS 0506738 to N.K.

Supporting Information is available on the WWW under http://www.small-journal.com or from the author.

Cu nanorods were deposited on a polished Cu substrate by oblique-angle deposition. Cu was selected for this study because it is widely used in heat-transfer applications.[19,20] In oblique-angle deposition, a flux of Cu atoms is incident on the substrate at a large incidence angle (>85°; see Figure 1a). This results in the formation of isolated nanorods due to the atomic shadowing effect[21,22] during growth, through which some of the incident atoms are not able to reach the substrate because of concurrent growth of parallel structures. Since the substrate was not rotated during the deposition process, the rods grew inclined[21] ($\alpha \approx 60^\circ$) towards the direction of the incident flux, as shown schematically in Figure 1a. The depositions were performed in an electron-beam evaporator with base pressure of $\approx 10^{-7}$ Torr.

Scanning electron microscopy (SEM) characterization was performed (Figure 1b) to study the structure of the deposited nanorods. The diameter of the nanorods increased from a few nanometers at the base to about 40–50 nm at the tip. The average tip-to-tip spacing between the nanorods is ≈50 nm and the nanorod height is ≈450 nm. The presence of defects (or voids) is also noticeable in the SEM image. These voids are an artifact of the uneven height distribution of the Cu substrate, which causes certain regions (for example, in valleys) to be shadowed out[22] during the oblique-angle deposition. These micrometer-scale voids give the Cu nanorod surface a combined nano- and microscale surface topography. The density of microscale defects on the Cu surface with nanorods ($\approx 10^4$ defects mm^{-2}) was comparable to that of the plain Cu surface.

Prior to performing the boiling heat-transfer experiments, we tested the wetting properties of the nanorod samples in comparison to the polished Cu substrate. For this, 2-μL droplets of distilled water were deposited on the substrates and the static contact angle was measured. The results (Figure 1c) indicate a reduction in the macroscopic water contact angle from approximately 55 to 38.5° due to the enhanced roughness[23] caused by the nanorod structures.

The test facility used to evaluate the effect of nanorod deposition on the boiling performance (Figure 2a) consists of a Cu block, liquid chamber, liquid supply system, and heating system. The Cu block is thermally insulated to assure nearly one-dimensional (1D) thermal conduction. Three K-type thermocouples (TC_1, TC_2, and TC_3; Figure 2a) are soldered onto the Cu block at a separation of 10 mm to monitor the temperature profile along the axial direction, and hence the 1D heat flux can be accurately estimated by Fourier Law.[24] The TC_1 sensor, which is ≈0.5 mm below the boiling surface, is used to estimate the heating wall temperature, while sensor TC_4 provides the ambient fluid temperature. The bubble visualization system comprises a Motion Scope high-speed charge-coupled device (CCD) camera with 640 × 480 resolution and a maximum frame rate of 2000 frames s^{-1}, an Olympus microscope (U-TV1X-2) with magnification from 60× to 1000×, and an Agilent data acquisition system. The Redlake image-processing program enables precise analysis of bubble release size and release frequency.

In the boiling tests, the power to the heater was increased and the process repeated until the critical heat flux (CHF) was

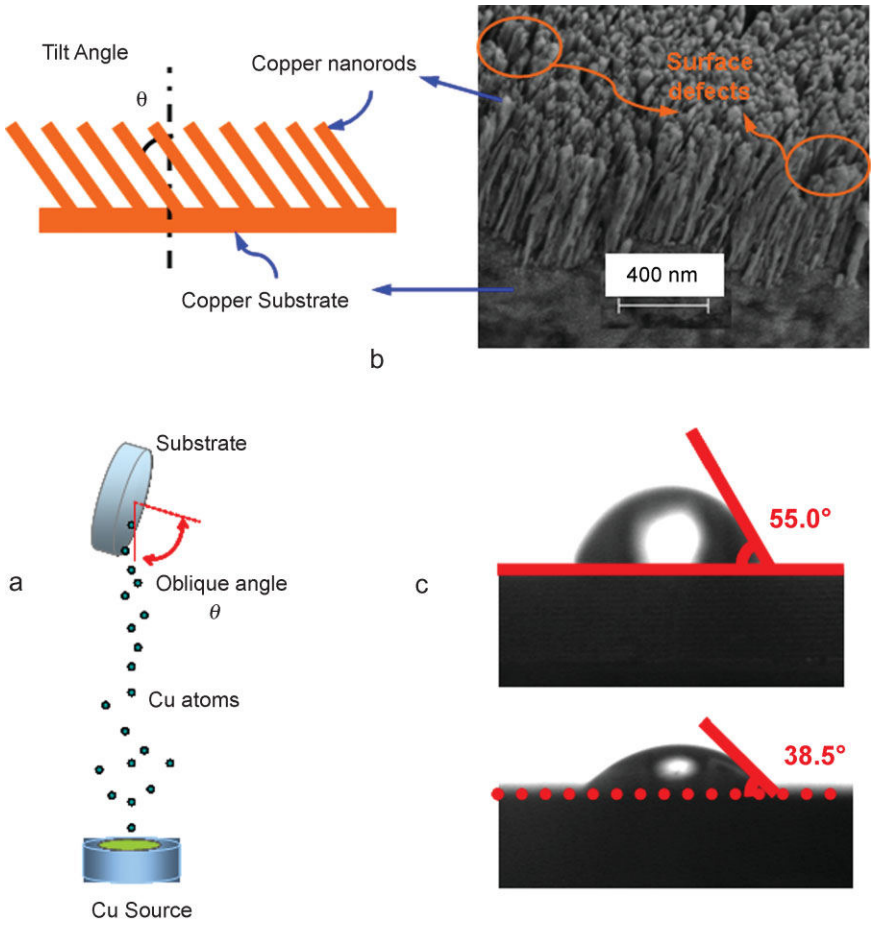

Figure 1. Nanostructured Cu surface. a) Bottom: the oblique-angle deposition process used to deposit the Cu nanorods on the planar Cu substrate; deposition was performed at an oblique incidence angle of ≈85°. Top: the substrate was not rotated during deposition, so the rods grew inclined towards the incident flux. b) SEM image of the Cu nanorods after deposition. The rods have an average diameter of ≈40–50 nm and are ≈450 nm in height. Surface defects or voids are also visible in the image, since the substrates on which the depositions were performed were not perfectly smooth. c) Water contact angle measurements for the Cu nanorod surface and the planar Cu substrate. The nanorods display an improvement in wettability.

achieved.[24] The data were categorized to obtain two key parameters: the superheat, $T_w - T_{sat}$ (T_w = wall temperature; T_{sat} = saturation temperature), and heat flux, q'' (including the CHF). These parameters are estimated (Supporting Information) from Fourier Law with the axial temperature profile and the known thermal conductivity of Cu. The uncertainty in the heat flux data was less than $\pm 5.5\ W\ cm^{-2}$ and less than $\pm 1.3\ ^{\circ}C$ for the superheat ($\Delta T_w = T_w - T_{sat}$). We quantified the heat-transfer performance through the boiling curve (i.e., the heat flux versus superheat surface temperature). The measured heat flux for the Cu nanorods was significantly higher (Figure 2b) than that for the Cu substrate without the depositions. Up to an order of magnitude increase in heat flux was achieved in the 7–12 K superheat range. The superheat for boiling incipience also decreased and the CHF was achieved at a significantly lower superheat. Over time the performance of the nanorod samples showed some degradation or aging. After repeated testing of the sample (indicated by #2 and #3 in Figure 2b), the heat flux was reduced but was still markedly superior to that of the plain Cu substrate without nanorods. This aging behavior is probably caused by oxidation and the accumulation of impurities.

To understand the mechanisms responsible for the improved boiling performance, we performed real-time visualization tests to study the dynamics of bubble formation and release on the nanostructured Cu surface and the baseline Cu surface (without nanorod deposition). To capture high-quality bubble images, the liquid was maintained in a slightly subcooled condition and the heat flux was increased stepwise from 4 to $25\ W\ cm^{-2}$. The bubble diameter and release frequency were measured using the Redlake imaging program and averaged over the boiling sites. The uncertainty of bubble size was primarily from the image resolution and less than ± 0.1 mm, and the bubble growth and waiting period was less than ± 1 ms. A detailed description of the imaging procedure used in this study is available in References [24] and [25]. The bubble release frequency and departure diameter for the Cu surface with nanorods are plotted as function of the wall superheat in Figure 3a and b, respectively. For comparison, data for the baseline Cu surface are also plotted. The release frequency and bubble diameter for the Cu

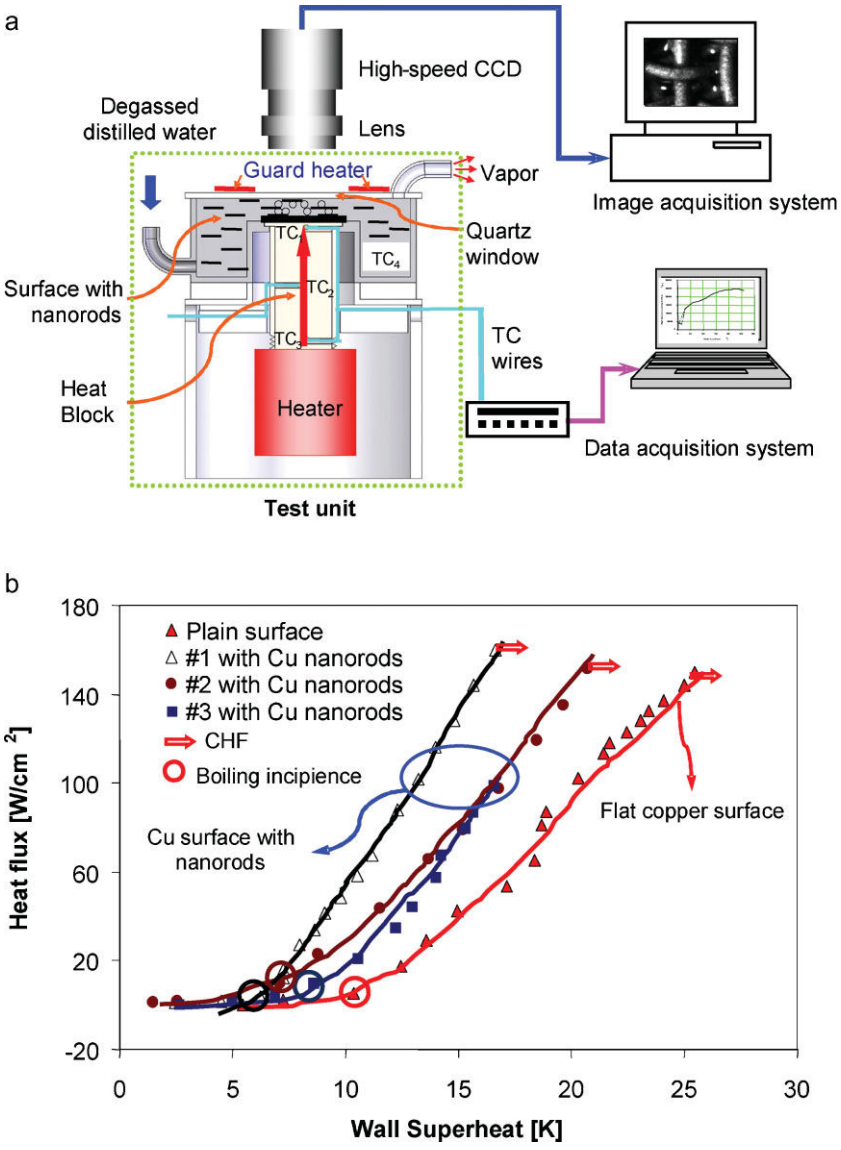

Figure 2. Boiling characterization tests. a) Schematic diagram showing the test setup composed of the test unit, data acquisition system, and visualization system. b) Boiling performance as a function of wall superheat. The red line indicates the boiling curve from an untreated Cu surface without nanorods. The other boiling curves are for three different tests performed on a typical Cu nanorod sample, and indicate significant improvement in heat flux coupled with lower boiling incipience and lower superheat to achieve CHF.

surface with nanorods show a nearly threefold difference compared with the baseline Cu surface. This finding indicates that the dynamics of bubble generation and release are fundamentally different for the surface with nanorods compared to conventional surfaces. The smaller bubble diameters and higher release frequencies may be related to the relatively small size of the microdefects (Figure 1b) and the enhanced wettability (Figure 1c) of the Cu surface with nanorods as compared to the plain Cu surface. Another very interesting observation was the high density of active bubble nucleate sites (Figure 3c) for the Cu surface with nanorods compared with the baseline Cu surface and with recently reported data[26,27] on Cu, brass, and stainless-steel surfaces without nanorods. Compared to uncoated surfaces, we observed an approximately 30-fold increase in nucleation site density for nanostructured Cu in the 5–10 K superheat range. This indicates that the bubble nucleation process is strongly influenced by the surface topography of the Cu nanorods.

The bubble diameter (D_b), bubble release frequency (f), and nucleation site density (N_a) are related to the average heat flux (q''_b) due to nucleate boiling[28] as follows:

$$q''_b = K\sqrt{\pi(k_l\sigma C_p)}fD_b^2N_a\Delta T_w \quad (1)$$

where k_l, C_p, and σ are the liquid thermal conductivity, specific heat, and surface tension, respectively. K is a constant that represents the bubble diameter of influence and is independent of the contact angle and physical properties of the fluid. Based on the data in Figure 3, the product of $\sqrt{f}D_b^2N_a$ [Eq. (1)] at low superheats

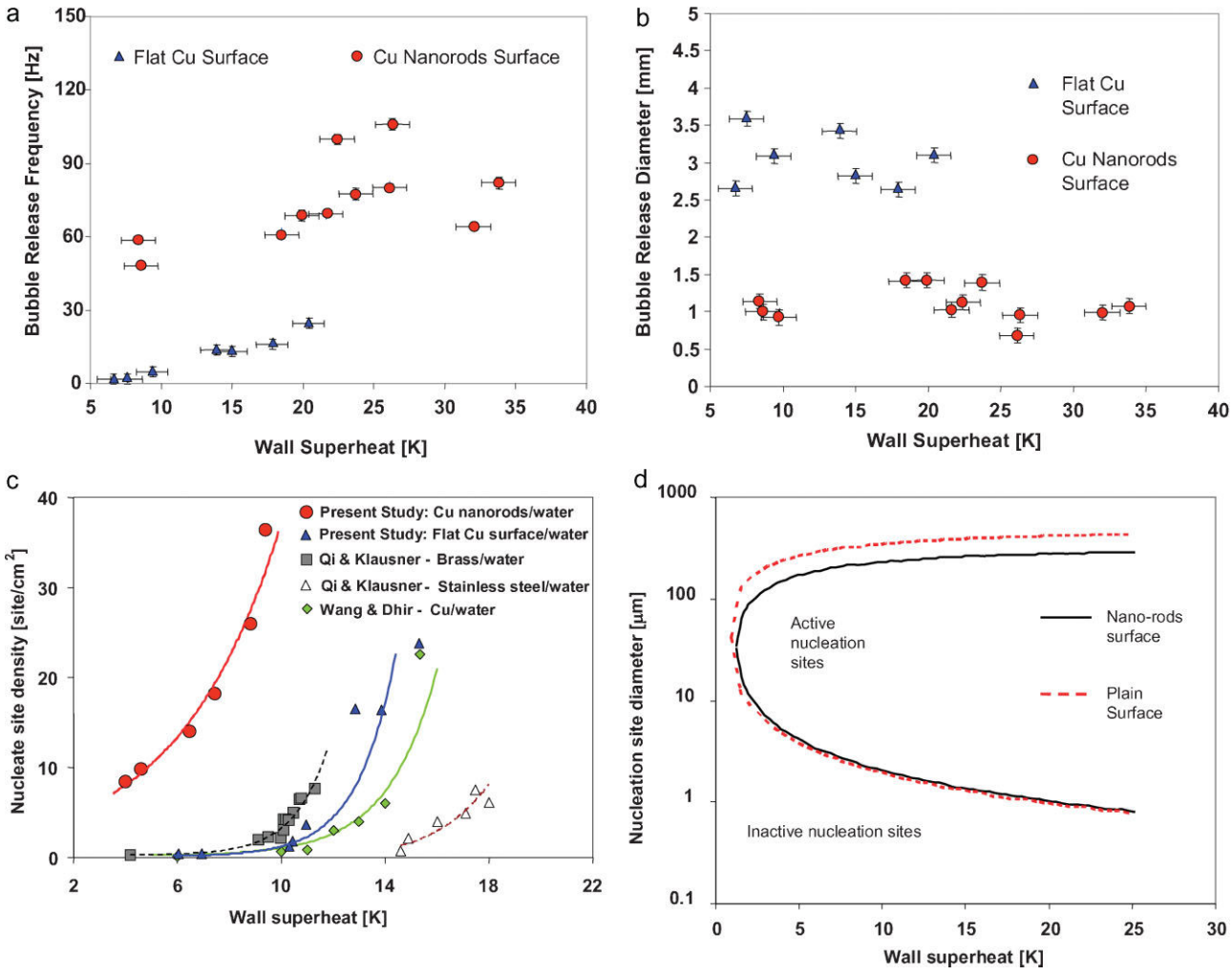

Figure 3. Bubble visualization study. a) Bubble release frequency as a function of wall superheat for the Cu surface with nanorods and the baseline Cu surface without nanorods. b) Corresponding results for the bubble release diameter as a function of wall superheat. c) The active nucleate site density for the surfaces with nanorods is ≈30-fold greater (in 5–10 K superheat range) than that for untreated surfaces. d) Predictions for the range of active cavity size as a function of wall superheat for the baseline Cu surface and the Cu surface with nanorods.

is about six times greater for Cu nanorods in comparison to planar Cu; this causes the heat-transfer performance to improve. The main mechanism responsible for this improvement is the nearly 30-fold increase (Figure 3c) in the nucleation site density (N_a) for the Cu nanorods. Bubble nucleation (i.e., the formation of vapor from metastable liquid) is directly related to the availability of vapor nuclei in the liquid or on the boundary surface. In the presence of a temperature gradient, the range of active nucleation sites that can trigger bubble growth is given by:[29]

$$\{D_{c,max}, D_{c,min}\} = \frac{\delta_t C_2}{2C_1} \frac{\Delta T_w}{\Delta T_w + \Delta T_{sub}} \times \left[1 \pm \sqrt{1 - \frac{8C_1 \sigma T_{sat}(\rho_l)(\Delta T_w + \Delta T_{sub})}{\rho_v h_{fg} \delta_t (\Delta T_w)^2}}\right] \quad (2)$$

where $D_{c,max}$ and $D_{c,min}$ are the maximum and minimum diameters of active surface cavities, respectively, and ρ_l and ρ_v are the liquid and vapor densities, respectively. $C_1 = 1 + \cos\theta$, $C_2 = \sin\theta$, θ is the contact angle, $\Delta T_{sub} = T_{sat} - T_f$, δ_t is the thermal boundary-layer thickness, T_f is the ambient liquid temperature, and h_{fg} is the latent heat of vaporization. Assuming a linear temperature profile in the liquid boundary layer, the thermal boundary-layer thickness δ_t can be simply expressed as: $\delta_t = \frac{k_l}{h_{sp}}$, where h_{sp} is the heat transfer coefficient in single-phase natural convection. For the present conditions, $h_{sp} \approx 500\ W\ m^{-2}\ ^\circ C$ and $\delta_t \approx 1$ mm. Figure 3d depicts the active nucleation site sizing obtained from Equation (2) for the untreated surface and the nanorod surface. The reduced contact angle of the surface with nanorods clearly cannot account for the reduction of the superheated temperature at onset of nucleate boiling and the increased density of active nucleation sites—in fact, the improved wettability of the nanorods suppresses the bubble ebullition process to higher surface temperatures. Figure 3d also shows that effective cavities that can readily trigger bubble nucleation need to maintain a gas/liquid interface with

radius of curvature on the micrometer scale. Therefore, a gas nanocavity formed in the nanopore between several nanorods cannot explain the significant improvement in the bubble nucleation density and frequency, and the subsequent enhancement of heat transfer.

Knowledge of the nucleation site stability provides insight into the processes governing the enhanced heat-transfer performance of the nanorod surface. Two important cavity traits dictate the tendency of a cavity to be active: the cavity diameter controls the superheat needed to trigger boiling, and the inner cavity characteristics determine its stability (i.e., its ability to contain air or vapor that forms and maintains the gas/liquid interface). It appears that in the surface with nanorods, the micrometer-sized surface defects or voids (Figure 1b) form favorable cavity sizes with mouth openings that can be readily activated at low superheated temperatures; the nanopores, created between the nanorods in the array, maintain the defect's stability. That is, the vapor pockets (or nanobubbles[16–18]) that are continuously generated within the cavities between the nanorods percolate through the porous nanorod network and feed the nucleation and growth of larger bubbles at the microscale defect sites. This enables stable nucleation to occur at very low superheats, as observed in the experiments. Without the stability provided by the nanopores, the micrometer-sized surface defects are unable to effectively trap air to form a gas/liquid interface and are readily flooded[13–15] upon introducing water or after a short operation at high heat fluxes. The inability of the naturally occurring microscale surface cavities of the plain surfaces (see Supporting Information) in the current work and other studies[26,27] to support low superheat temperatures is strongly indicative of the ability of the interconnected network of nanopores to effectively trap vapor/air and maintain the microcavity stability.

In the conventional scale, enhanced boiling surfaces[13–15] consist of cavities with a mouth (that controls the superheat needed to initiate boiling) and a reentrant cavity (that provides the stability for prolonged operation). However, unlike macro surfaces in which the inner cavity dimensions are typically larger than the mouth diameter, in the nano surface the cavity stability is provided by features with orders-of-magnitude smaller scales than the mouth opening. In this way, activation of multiple scales from nano to micro plays a key role in enhancing the nucleate boiling performance of the Cu surface with nanorods. While this study was focused on Cu, the concept of activating the solid/liquid/gas interface at multiple scales to generate significant improvements in nucleate boiling may also be applicable to other metals and interfaces. The oblique-angle deposition scheme that was used to deposit the Cu nanorods can be readily adapted to create nanostructures from a range of different materials or even a combination of materials. As such, these devices can have a broad impact in thermal and chemical processes that involve boiling, for example, the design of two-phase heat exchangers for energy harvesting and thermal management of high heat flux in Cu interconnects and semiconductor devices.

Keywords:

copper · heat transfer · interfaces · nanorods · nucleate boiling

[1] J. R. Thome, *Int. J. Heat Fluid Flow* **2004**, *25*, 128.
[2] W. Frank, *Nature* **1998**, *395*, 220.
[3] P. Cheng, H.-Y. Yu, F.-J. Hong, *J. Heat Transfer* **2007**, *129*, 101.
[4] J. L. McGrew, F. L. Bamford, T. R. Rehm, *Science* **1966**, *153*, 1106.
[5] J. Lee, I. Mudawar, *Int. J. Heat Mass Transfer* **2005**, *48*, 928.
[6] S. Daniel, M. K. Chaudhury, J. C. Chen, *Science* **2001**, *291*, 633.
[7] J. H. Kim, K. N. Rainey, S. M. You, J. Y. Pak, *J. Heat Transfer* **2002**, *124*, 500.
[8] C.-J. Kuo, A. Kosar, Y. Peles, S. Virost, C. Mishra, M. K. Jensen, *J. Microelectromech. Syst.* **2006**, *15*, 1514.
[9] L. Jiang, M. Wong, Y. Zohar, *J. Microelectromech. Syst.* **2001**, *10*, 80.
[10] A. E. Bergles, M. C. Chyu, *J. Heat Transfer* **1982**, *104*, 279.
[11] S. S. Mehendale, A. M. Jacobi, R. K. Shah, *Appl. Mech. Rev.* **2000**, *53*, 175.
[12] S. G. Liter, M. Kaviany, *Int. J. Heat Mass Transfer* **2001**, *44*, 4287.
[13] V. P. Carey, *Liquid–Vapor Phase-Change Phenomena: An Introduction to the Thermophysics of Vaporization and Condensation Processes in Heat Transfer Equipment*, Taylor & Francis, London **1992**.
[14] L. S. Tong, Y. S. Tang, *Boiling Heat Transfer and Two Phase Flow*, Taylor & Francis, London 1997.
[15] P. G. Debenedetti, *Metastable Liquids*, Princeton University Press, NJ **1996**.
[16] R. E. Cavicchi, C. T. Avedisian, *Phys. Rev. Lett.* **2006**, *98*, 124501.
[17] J. W. G. Tyrrell, P. Attard, *Phys. Rev. Lett.* **2001**, *87*, 176104.
[18] M. Holmberg, A. Kuhle, J. Garnaes, K. A. Morch, A. Boisena, *Langmuir* **2003**, *19*, 10510.
[19] G. Chen, *Nanoscale Energy Transport and Conversion: A Parallel Treatment of Electrons, Molecules, Phonons and Photons*, Oxford University Press, Oxford **2005**.
[20] P. Reddy, S.-Y. Jang, R. A. Segalman, A. Majumdar, *Science* **2007**, *315*, 1568.
[21] Y.-P. Zhao, D.-X. Ye, G.-C. Wang, T.-M. Lu, *Nano Lett.* **2002**, *2*, 351.
[22] R. Tekir, T. Karabacak, T.-M. Lu, N. Koratkar, *Appl. Phys. Lett.* **2006**, *89*, 193116.
[23] S. J. Kim, I. C. Bang, J. Buongiorno, L. W. Hu, *Appl. Phys. Lett.* **2006**, *89*, 153107.
[24] C. Li, G. P. Peterson, Y. Wang, *J. Heat Transfer* **2006**, *128*, 1312.
[25] J. Li, G. P. Peterson, *Int. J. Heat Mass Transfer* **2005**, *48*, 4316.
[26] C. H. Wang, V. K. Dhir, *J. Heat Transfer* **1993**, *115*, 659.
[27] Y. Qi, J. Klausner, *J. Heat Transfer* **2006**, *128*, 13.
[28] B. B. Mikic, W. M. Rohsenow, *J. Heat Transfer* **1969**, *91*, 245.
[29] Y. Y. Hsu, *J. Heat Transfer* **1962**, *84*, 207.

Received: October 17, 2007
Published online: June 23, 2008

